

Article

Restoring the Oxidase-Like Activity of His@AuNCs for the Determination of Alkaline Phosphatase

Fanfan Xiao ^{1,†}, Yuting Yu ^{1,†}, Yang Wu ¹, Lili Tian ¹, Guoyan Zhao ¹, Hailong Pang ¹ and Jie Du ^{1,2,*} 

¹ College of Life Sciences, Northwest Normal University, Lanzhou 730070, China; 2018212256@nwnu.edu.cn (F.X.); 2017212141@nwnu.edu.cn (Y.Y.); 2020212651@nwnu.edu.cn (Y.W.); 2018212262@nwnu.edu.cn (L.T.); 2018212254@nwnu.edu.cn (G.Z.); Phl-3088@163.com (H.P.)

² Key Laboratory of Bioelectrochemistry & Environmental Analysis of Gansu Province, Northwest Normal University, Lanzhou 730070, China

* Correspondence: dujie@nwnu.edu.cn

† These authors contributed equally to this work.

Abstract: In this paper, we propose a simple colorimetric method for the sensitive and selective detection of alkaline phosphatase (ALP) activity based on the turn off/turn on oxidase mimic activity of His@AuNCs. His@AuNCs/graphene oxide hybrids (His@AuNCs/GO) were easily obtained using the self-assembly method with poly (diallyldimethylammonium chloride) (PDDA)-coated GO and showed high oxidase-like activity compared with His@AuNCs. We found that the pyrophosphate ion ($P_2O_7^{4-}$, PPI) could effectively inhibit the oxidase mimic activity of His@AuNCs/GO, and the hydrolysis of PPI by ALP restored the inhibited activity of His@AuNCs/GO, enabling them to efficiently catalyze the oxidation of 3,3',5,5'-tetramethylbenzidine (TMB) to generate the blue oxidized product oxTMB. The intensity of the color showed a linear dependency with the ALP activity. ALP was detected in the linear range of 0–40 mU/mL with a low detection limit (LOD) of 0.26 mU/mL ($S/N = 3$). The proposed method is fast, easy, and can be applied to monitor the ALP activity in serum samples accurately and effectively, which suggests its practicability and reliability in the detection of ALP activity in clinical practice.

Keywords: His@AuNCs/GO; oxidase-like activity; PPI; ALP; colorimetric detection



Citation: Xiao, F.; Yu, Y.; Wu, Y.; Tian, L.; Zhao, G.; Pang, H.; Du, J.

Restoring the Oxidase-Like Activity of His@AuNCs for the Determination of Alkaline Phosphatase. *Biosensors* **2021**, *11*, 174. <https://doi.org/10.3390/bios11060174>

Received: 27 April 2021

Accepted: 26 May 2021

Published: 30 May 2021

Publisher's Note: MDPI stays neutral with regard to jurisdictional claims in published maps and institutional affiliations.



Copyright: © 2021 by the authors. Licensee MDPI, Basel, Switzerland. This article is an open access article distributed under the terms and conditions of the Creative Commons Attribution (CC BY) license (<https://creativecommons.org/licenses/by/4.0/>).

1. Introduction

Alkaline phosphatase (ALP) is widely present in the tissues and organs of biological organisms (e.g., bones, liver, intestine, kidneys, and placenta) and can catalyze the hydrolysis and transphosphorylation of a variety of phosphate compounds, including DNA, proteins, and other small molecules [1,2]. Several diseases, such as bone cancer [3], prostate cancer [4], and diabetes [5] and liver diseases [6], are influenced by ALP activity, and thus it has been recognized as a significant biomarker in medical diagnostics.

ALP is frequently utilized as an enzyme label in biochemical assays, such as the enzyme-linked immunosorbent assay (ELISA) [7]. Therefore, simple, sensitive, and reliable assays are highly desirable in the detection of ALP activity in the research and diagnosis of diseases [8–10]. Several conventional methods are typically used for ALP activity determination, such as electrochemistry [11,12], fluorometry [13,14], colorimetry [15,16], etc.

Among these, the colorimetric method has spurred great interest owing to its intrinsic simplicity, speed, and cost-effectiveness. In the standard method that is often employed, colorless *p*-nitrophenyl phosphate (pNPP) is used as the substrate and is converted into the yellow *p*-nitrophenolate using ALP as the catalyst, and the reaction results in realistic colorimetric assays [17]. However, previous colorimetric methods often showed inferior sensitivity and reproducibility, as direct measurement of the subtle color change of the substrates or products of ALP was extremely difficult [18]. To address this shortfall, the

cascading of an additional amplification process to establish the sensitivity of ALP is of value.

Research studies have reported that using the substrates or products of ALP to regulate plasmonic gold and silver nanomaterials [19–21] helped to achieve signal amplification. For example, using plasmonic gold nanorods, Gao et al. designed a colorimetric assay to determine the ALP activity. In this method, ALP was used as the catalyst in the hydrolysis of ascorbic acid-2-phosphate (AA-P) to ascorbic acid (AA); the AA was then used to reduce the silver ions to generate a silver shell on the Au nanoclusters (AuNCs), which led to a perceptible color change producing the signal readout [14].

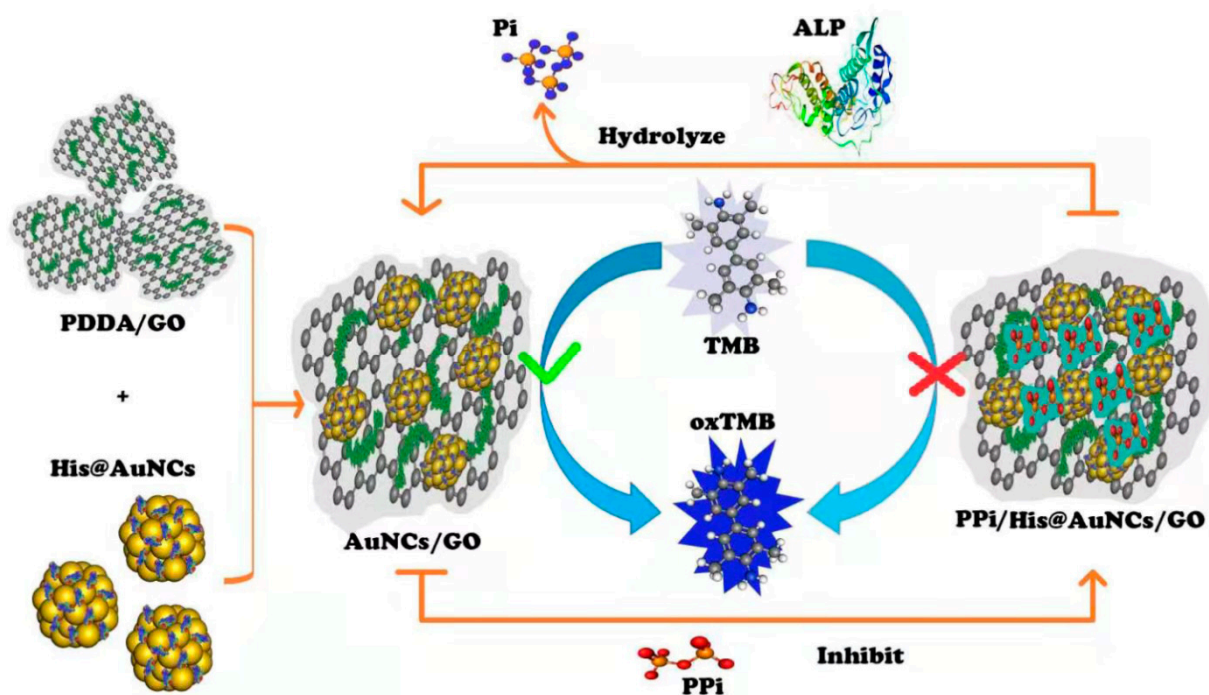
Although these approaches can provide a simple and visual detection of ALP, plasmonic nanomaterials suffer from non-specificity of ions in complex biological samples [22], resulting in poor sensitivity and a limited linear range. Recently, alternative strategies, using the substrates and products of ALP, have been developed to modify nanozymes (nanomaterials with intrinsic enzyme-like properties), which could result in signal amplification [23,24].

For example, Tian et al. reported an ALP assay employing MnO₂ nanosheets as the signal amplifier [25]. The MnO₂ nanosheets catalyze the oxidation of the colorless substrate TMB to form the blue oxidized product (oxTMB) and ALP catalyzes the hydrolysis of AA-P to AA, which could weaken the activity of the MnO₂ nanosheets, subsequently weakening the MnO₂-controlled cascade signal. As a result, the readout signal amplification corresponding to the ALP activity can be obtained from the change in absorption. Chen et al. also developed a nanozyme-based signal amplification method by modifying the catalytic activities of gold nanoclusters (AuNCs) for the colorimetric detection of ALP activity [26].

These nanozyme-based ALP activity assays can achieve signal amplification [27–29]. Some methods can even be efficiently used in colorimetric immunoassays. However, the sensitivities of these methods are highly dependent on the enzyme-like catalytic activity of the nanozymes. Usually, the catalytic activities of nanozymes are low when compared with those of natural enzymes, which limits their application. Therefore, the sensitivity of nanozyme-based ALP assays must be enhanced by improving the catalytic activities of the nanozymes.

Anchoring NPs on suitable nanoscale supporters to form hybrid nanomaterials has recently been found to be an effective method to enhance the catalytic activity of nanozymes [30–34]. Studies have reported that the enzyme-like activity of metal NCs can be greatly enhanced by decorating them on two-dimensional nanomaterials, such as graphene and graphitic carbon nitride. For instance, Wu et al. demonstrated that AuNPs grown in situ on g-C₃N₄ nanosheets are hybrid nanozymes, have higher catalytic activities than both C₃N₄ nanosheets and AuNPs, and can be applied in the colorimetric detection of glucose [35]. Chen et al. constructed a colorimetric hydrogen peroxide (H₂O₂) sensor using TMB in an acetate buffer (pH 4) solution, based on Fe/Pt nanoparticles decorated on graphene oxide (GO) nanosheets as oxidase mimics [36]. In our recent work, we improved the catalytic activity of histidine-protected AuNCs (His@AuNCs) by decorating the nanoclusters on reduced graphene oxide (RGO), with the nitrite modulating the oxidase mimic activity of the His@AuNCs, thus, leading to the development of a nitrite sensor [37].

In this work, a novel nanozyme-based colorimetric platform for the simple, sensitive, and selective screening of ALP activity was successfully developed. As shown in Scheme 1, His@AuNCs can be efficiently decorated on poly (diallyldimethylammonium chloride) (PDDA)-functionalized GO using a facile sequential process, and the resulting His@AuNCs/GO with improved oxidase-like performance can be used to effectively catalyze TMB to oxTMB. Interestingly, the catalytic activity of His@AuNCs/GO dramatically decreased with the presence of pyrophosphate ion (PPi) in the buffer solution.



Scheme 1. Illustration of the colorimetric sensing strategy for ALP activity based on PPI-mediated catalytic activity of His@AuNCs/GO.

In the presence of ALP, PPI is hydrolyzed to phosphate (Pi), resulting in the restoration of the catalytic activity of His@AuNCs/GO, enabling the detection of the ALP activity. The proposed method shows a good linear relationship in the range of 0–40 mU/mL with a LOD of 0.26 mU/mL. In addition, ALP in human serum samples was detected successfully using this method, which indicates its potential as a promising candidate in biological and biomedical applications.

2. Materials and Methods

2.1. Chemicals and Instruments

L-Histidine (His), ALP, and TMB were purchased from Aladdin Chemistry Co., Ltd. GO was purchased from Nanjing XFNano Mstar Technology, Ltd. (Nanjing, China). Sodium pyrophosphate tetrabasic decahydrate ($\text{Na}_4\text{P}_2\text{O}_7 \cdot 10\text{H}_2\text{O}$) and PDDA (MW = 400,000–500,000, 20 wt% in water) were purchased from Sigma-Aldrich (Shanghai, China). Chloroauric acid tetrahydrate (HAuCl_4), poly(N-vinyl-2-pyrrolidone) (PVP) (K30, MW = 30,000–40,000), KCl, and other chemicals were purchased from Sinopharm Chemical Reagent Co. Ltd. (Shanghai, China). Dialysis bags (molecular weight cut-off (MWCO) of 1000 Da; regenerated cellulose (RC) membranes) were purchased from Shanghai Yuanye Bio-Technology Co., Ltd. (Shanghai, China). All chemicals were of analytical grade and were directly used without further purification. All solutions were prepared with deionized water (18.25 M Ω cm).

We used transmission electron microscopy (TEM) by a TECNAI G² field emission projection electron microscope (FEI TECNAI G20, Waltham, MA, USA). We used a Nicolet iS50 Fourier transform infrared spectroscope (Thermo Scientific, Waltham, MA, USA) for infrared spectra collection. We obtained all absorption spectra on a UV-1800 ultraviolet-visible spectrophotometer (Shimadzu, Japan). We used a pH meter (Sartorius AG, Germany) for pH adjustment.

2.2. Synthesis of His@AuNCs

His@AuNCs were prepared based on a previous work by our group [37]. In this method, an aqueous solution of HAuCl_4 (1 mL, 10 mM) was blended with an aqueous

solution of histidine (3 mL, 0.15 mM) and the mixture was incubated for 2 h at 25 °C. The color of the mixture changed from light yellow to light brown; when the mixture was irradiated with 365 nm ultraviolet light, the mixture emitted a strong blue light. The His@AuNCs solution that was obtained was isolated from the precipitates by centrifugation at 14,000 rpm for 15 min and then washed using a dialysis bag (MWCO: 1000 Da) until the pH of the solution became neutral. The His@AuNCs obtained were concentrated by freezing and drying under vacuum, were re-dispersed in an aqueous solution, and were stored at 4 °C until further use.

2.3. Synthesis of His@AuNCs/GO

First, PDDA/GO was prepared according to the literature, with a slight modification [38]. In this method, 40 mg PVP was added to 10 mL GO solution (0.25 mg/mL) and sonicated for 30 min. The resulting black solution was washed, centrifuged three times, and dissolved in 2.5 mL of water. Afterwards, 0.05 mL of 20 wt% PDDA was mixed well with 8.4 mL of 0.625 M KCl, followed by the injection of 2.1 mL PVP-capped GO; the resulting solution was sonicated for 1.5 h.

The black sediment was washed with deionized water and subjected to centrifugal separation. Finally, the products were re-dispersed in 2 mL water and named as PDDA/GO. For the fabrication of His@AuNCs/GO, 1 mL PDDA/GO (1 mg/mL) was added to 40 mL of the His@AuNCs solution under stirring (Figure S1). The solution was then sonicated for 3 min before being left to stand overnight, then washed three times, and dissolved in 2 mL water (final concentration: 0.5 mg/mL). This His@AuNCs/GO solution (0.005 mg/mL, Figure S2) was used for the subsequent experiments

2.4. Oxidase-Like Activity of His@AuNCs/GO

The oxidase-like activity of His@AuNCs/GO was tested using TMB as the substrate. Similarly, we used His@AuNCs instead of His@AuNCs/GO to conduct control experiments under the same conditions. For the subsequent experiments, 10 µL His@AuNCs/GO (0.5 mg/mL) was added to 1000 µL of the total reaction solution. Based on the maximum concentration of oxTMB, the other experimental parameters were optimized as follows (Figure S3): (1) the pH and concentration of acetate buffer were maintained at 3.2 and 50 mM, and (2) the concentrations of TMB was fixed at 1.6 mM. In detail, 100 µL of TMB (1–18 mM) and 10 µL of the pre-prepared His@AuNCs/GO (0.5 mg/mL) were added to 890 µL (pH 3.2, 50 mM) of acetate buffer and mixed thoroughly. After incubating at 25 °C for 5 min, the UV–visible spectrum was measured with a spectrophotometer.

We used the Lineweaver–Burk equation to calculate the kinetic parameters (V_{\max} and K_m) [39]:

$$v = \frac{V_{\max} \times [S]}{K_m + [S]}, \quad (1)$$

where v is the reaction velocity, $[S]$ is the concentration of the substrate, V_{\max} is the maximum reaction velocity, and K_m is the Michaelis–Menten constant [40].

2.5. Inhibiting of the Oxidase-Like Activity of His@AuNCs/GO by PPI

To check the inhibiting ability of PPI, 10 µL $\text{Na}_4\text{P}_2\text{O}_7 \cdot 10\text{H}_2\text{O}$ stock solution with different concentrations (0–6 mM) was added to 10 µL His@AuNCs/GO (0.5 mg/mL) and incubated at 25 °C for 10 min. The resultant solution was added to a solution containing 100 µL TMB (16 mM), and 880 µL of acetate buffer (pH 3.2, 50 mM) and stirred for 5 min at 25 °C. The UV–vis spectrum of the resultant solution was collected using a spectrophotometer.

2.6. Colorimetric Detection of ALP Activity

To determine the ALP activity, it is necessary to mix 10 µL of 4 mM PPI and freshly prepared ALP solutions of different concentrations, dilute to 100 µL with 0.05 M Tris-HCl buffer (pH 7.4), and incubate at 37 °C for 30 min (The incubation time was optimized to

30 min, Figure S4) [41]. Next, the above solutions and 10 μL His@AuNCs/GO (0.5 mg/mL) were mixed and incubated at room temperature for 10 min. The subsequent experimental steps were the same as those mentioned in Section 2.5 (final concentration of PPI: 40 μM).

To evaluate the practical application of our proposed method, ALP in human serum samples was used for spiked experiments. Typically, human serum samples obtained from school hospital of Northwest normal university. The serum samples were diluted 50-fold with deionized water, and we performed the spike experiment with a known ALP concentration of 1 to 10 mU/mL.

3. Results

3.1. Characterization of His@AuNCs/GO

TEM was employed for the characterization of the morphology of His@AuNCs and His@AuNCs/GO. A typical TEM image (Figure 1A) showed that the His@AuNCs were highly uniform and monodisperse with a narrow size distribution of 1.72 nm (the size was statistically calculated from more than 100 NCs in the TEM image (Figure S5)). In addition, the high-resolution transmission electron microscopy (HR-TEM) revealed a high crystallinity of the resulting His@AuNCs.

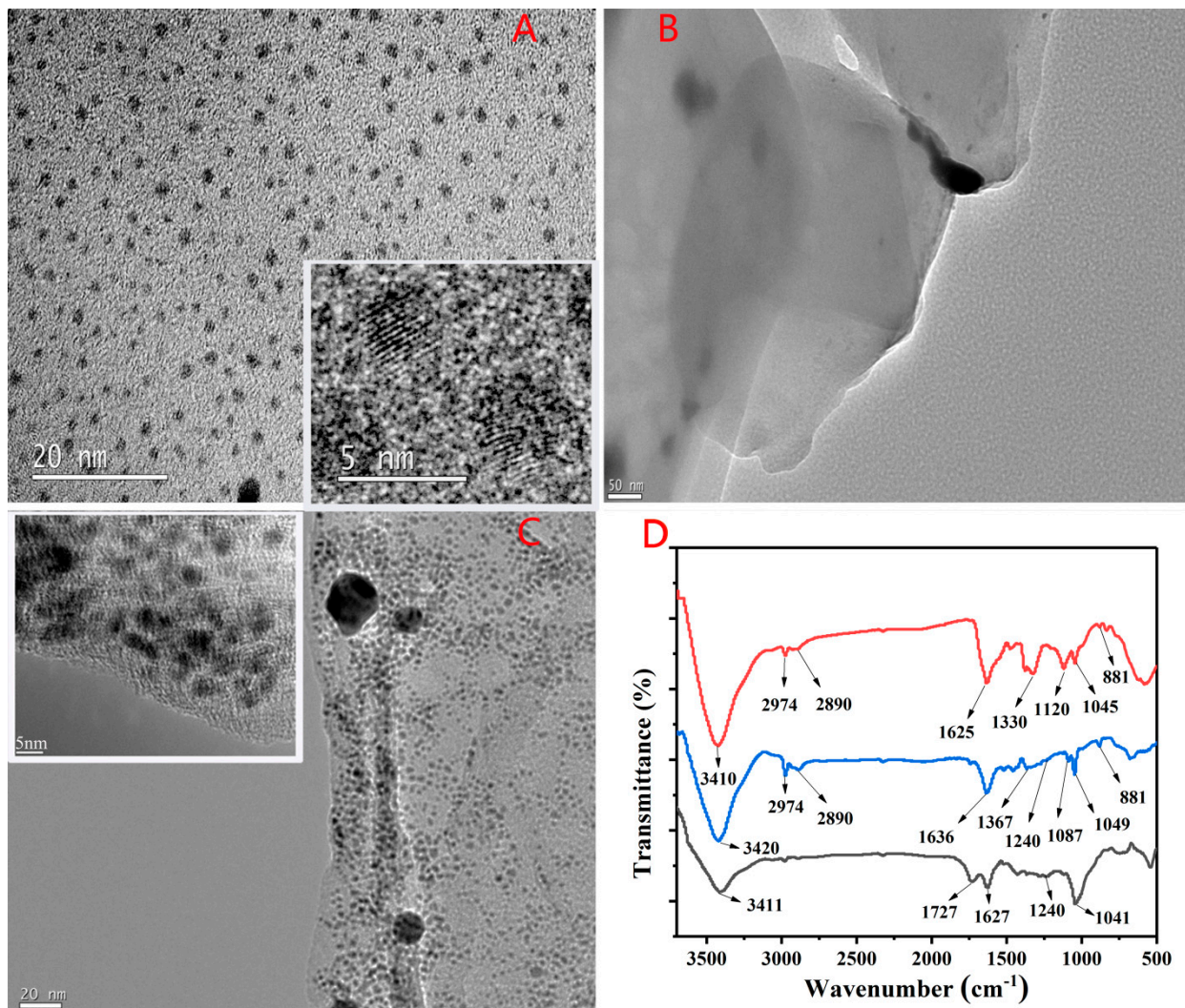


Figure 1. Characterization of His@AuNCs, GO, and His@AuNCs/GO, respectively. (A) TEM of His@AuNCs, (B) TEM of GO, (C) TEM of His@AuNCs/GO, (D) FT-IR spectra of GO (black), His@AuNCs (red) and His@AuNCs/GO (blue). Insert in (A), (C) show HR-TEM of His@AuNCs and His@AuNCs/GO, respectively.

As can be seen in Figure 1A (inset), the His@AuNCs showed clear lattice fringes with an interplanar distance of 0.24 nm, corresponding to the (111) lattice planes of the face-centered cubic structure of metallic Au (Figure 1A, inset). Figure 1B,C, respectively, shows the typical images before and after the loading of the His@AuNCs onto PDDA/GO. It may be observed (Figure 1C) that the GO nanosheets were modified by His@AuNCs. To further characterize, the FTIR spectra of GO, His@AuNCs and His@AuNCs/GO were recorded (Figure 1D). It can be observed that the characteristic peaks of GO (1041, 1240 cm^{-1}) and His@AuNCs (881, 1330, 2974, 2890 cm^{-1}) appear in His@AuNCs/GO at the same time [42,43]. Besides, Figure S6 shows EDX analysis of the GO, His@AuNCs, and His@AuNCs/GO, and the presence of the elements C, N, O, and Au were detected in His@AuNCs/GO. These results demonstrate that His@AuNCs effectively self-assembled on the PDDA/GO platform to form His@AuNCs/GO.

3.2. Oxidase-Like Activity of His@AuNCs/GO

In our recent work, the oxidase mimic activity of His@AuNCs was studied by the catalytic oxidation of the substrate TMB [37]. In this work, the oxidase-like activity of the His@AuNCs loaded onto PDDA/GO was investigated. As shown in Figure 2A, compared with the His@AuNCs-TMB system, a visible color change was observed in the His@AuNCs/GO-TMB system (inset of Figure 2A). This result was also evidenced by the UV-vis absorption spectrum at 652 nm. The results indicated that His@AuNCs/GO has an oxidase-like activity. We further studied the catalytic properties of His@AuNCs/GO through steady-state kinetic experiments.

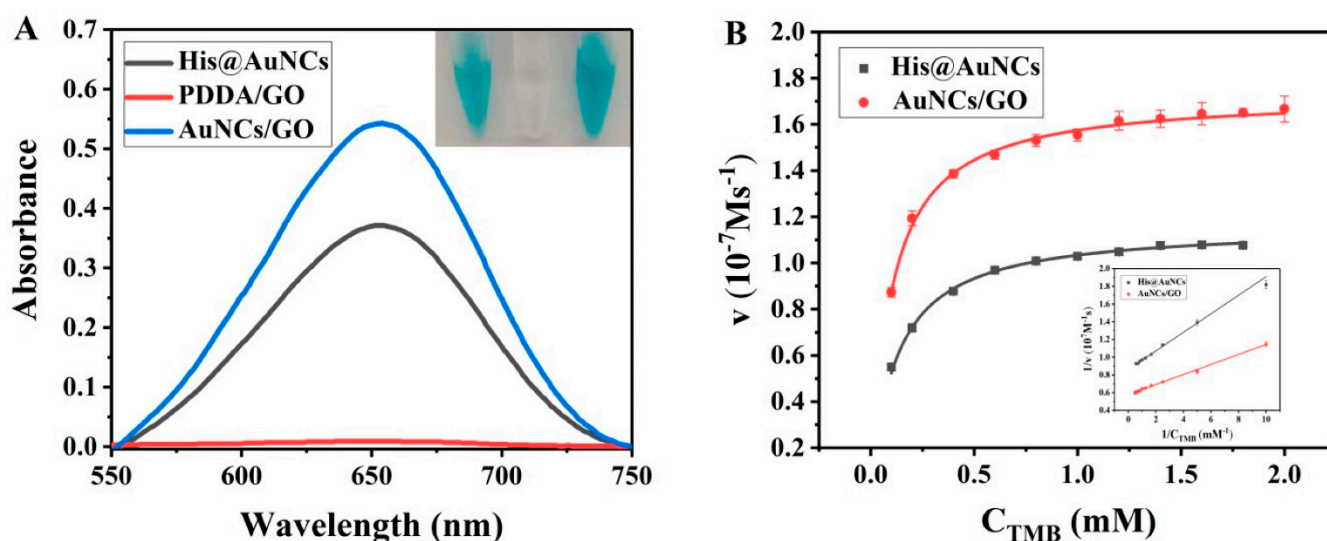


Figure 2. (A) The UV-vis absorption spectra of His@AuNCs, PDDA/GO, and His@AuNCs/GO in the colorimetric system with TMB as a substrate. The inset shows the corresponding photographs. Inset: photograph of corresponding solution (from left to right: His@AuNCs, PDDA/GO, and His@AuNCs/GO). (B) Michaelis–Menten curve of nanomaterials (His@AuNCs, His@AuNCs/GO) with different concentrations of TMB (inset: the Lineweaver–Burk plot of nanomaterials with different concentrations of TMB).

As seen in Figure 2B, the initial rate versus TMB concentration followed typical Michaelis–Menten behaviors for a certain range of substrate concentrations. Under the same conditions, the absorption of the His@AuNCs-TMB solution was further investigated. The K_m and the V_{max} were calculated using the Lineweaver–Burk plot [37]: the K_m and V_{max} of His@AuNCs/GO were found to be 0.098 mM and $1.728 \times 10^{-7} \text{ M s}^{-1}$, respectively, and those of His@AuNCs were found to be 0.126 mM and $1.164 \times 10^{-7} \text{ M s}^{-1}$, respectively (Table 1). The results indicated that His@AuNCs/GO in comparison with His@AuNCs had a higher affinity toward TMB, that is, a better oxidase-like catalytic activity.

Table 1. Apparent steady-state kinetics parameter for nanomaterials oxidase mimic activity.

Catalyst	K_m (mM)	V_{max} (10^{-7} M s $^{-1}$)
His@AuNCs (TMB)	0.126	1.164
His@AuNCs/GO (TMB)	0.098	1.728

3.3. Inhibitory Effects of PPI

As the proposed method was based on the modulation of the oxidase-like activity of His@AuNCs/GO, we first investigated the inhibitory effects of PPI on the activities of His@AuNCs/GO. Different amounts of PPI and His@AuNCs/GO were mixed and added into the catalytic oxidation reaction solution containing TMB. The typical absorption spectra around 652 nm are shown in Figure 3A. Figure 3B shows the dose-related inhibitory ability of PPI on the oxidase-like activity of His@AuNCs/GO; the absorption signals were linear with the PPI observed within the range of 0–40 μ M ($Y = -0.012X + 0.542$, $R^2 = 0.985$). As the maximum inhibition of the catalytic activity occurred when 40 μ M of PPI was added, the concentration of 40 μ M was selected for subsequent detection. Moreover, the inhibitory effects of PPI to the oxidase-like activity of His@AuNCs were investigated. As shown in Figure S7, the inhibitory effects of PPI to the His@AuNCs are far lower than that to His@AuNCs/GO, indicating that His@AuNCs/GO is needed in the proposed method.

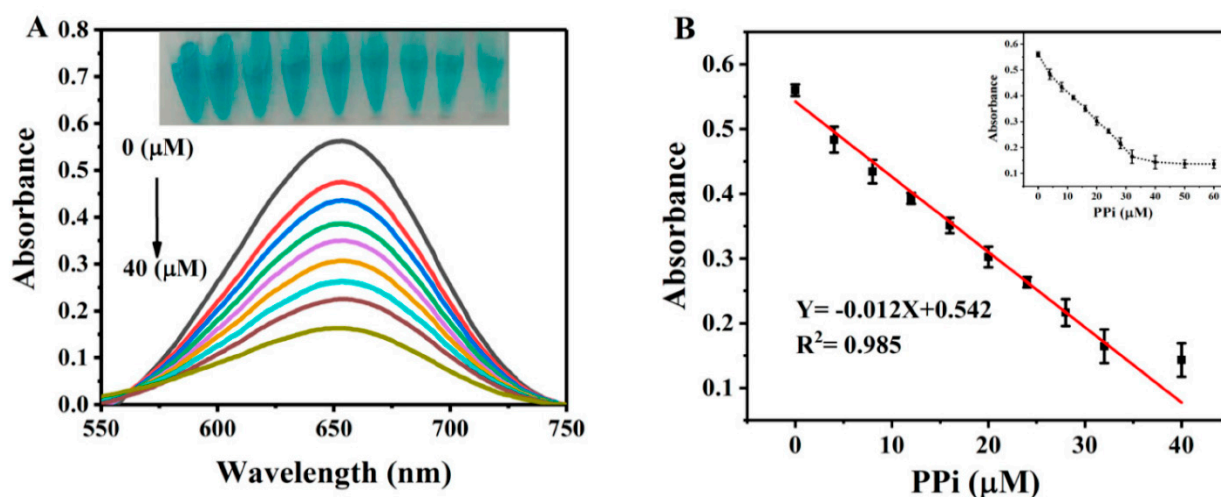


Figure 3. (A) The UV-vis absorption spectra of the His@AuNCs/GO-TMB system in the presence of various concentrations of PPI. Inset shows the photos of the corresponding solutions. (B) Linear relationship for PPI detection. Absorbance changes with the increase of PPI concentration from 4 to 60 μ M (inset). Error bars represent the standard deviations ($n = 3$).

According to the previous reports about nanozymes, in the presence of reducing agents, TMB is less effectively oxidized, which may be due to different mechanisms—namely, reducing oxTMB to colorless TMB [44–46]. To clearly explain the inhibitory behavior of PPI, we explored whether PPI can reduce oxTMB. Figure S8 shows the absorbance at 652 nm when PPI is added to the His@AuNCs/GO-TMB system after 5 min of chromogenic reaction. Compared with the system without PPI, there was no obvious change in absorbance, which proves that PPI cannot reduce oxTMB. Therefore, we suggest that the inhibition of PPI to His@AuNCs/GO is similar to previous reports [47,48], as shown in Scheme 1, as PPI has strong affinities toward His@AuNCs/GO [49,50].

3.4. Detection of ALP Activity

ALP can catalyze the hydrolysis of PPI in a weak medium to generate Pi. Thus, we hypothesize that it is possible to restore the inhibited activity of nanozymes when ALP is incubated with PPI/His@AuNCs/GO (His@AuNCs/GO treated with PPI) via the hydrolysis of PPI. With this assumption, we designed a colorimetric ALP activity assay (Scheme 1), and evaluated the sensitivity of the colorimetric analysis in the detection of the ALP activity.

Figure 4A shows the absorption spectra of the ALP-treated PPI/His@AuNCs/GO-TMB system with different concentrations of ALP. The absorption signal increased with increasing ALP concentration.

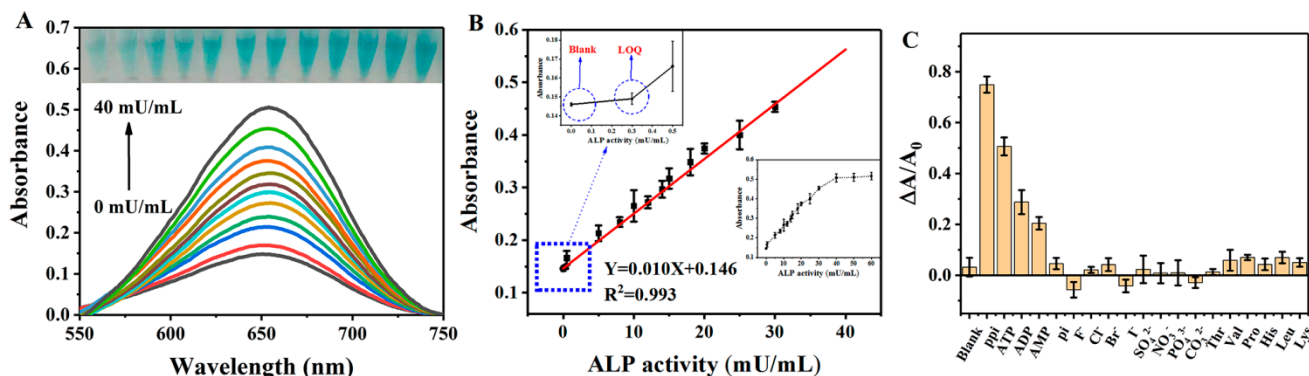


Figure 4. (A) The UV–vis absorption spectra of the His@AuNCs/GO-TMB system in the absence and presence of various concentrations of ALP; the inset shows the photos of corresponding solutions. (B) Linear relationship between the absorbance at 652 nm and the ALP concentration. Absorbance changes with the increase of ALP concentration from 0.5 to 60 mU/mL (inset). Error bars represent the standard deviations ($n = 3$) (C) Selectivity of the assay for PPI compared to other potential interferences. Experimental conditions: PPI (40 μ M), other anions (200 μ M), and amino acids (500 μ M). Error bars represent the standard deviations ($n = 3$).

To verify whether Pi and ALP are directly involved in the restoration of the inhibited catalytic activity of His@AuNCs/GO, we performed control experiments by adding Pi and ALP to the His@AuNCs/GO-TMB system. As seen in Figure S9, no color change was seen in the control tests. The results confirmed the feasibility of the proposed strategy for ALP activity sensing (Scheme 1). Under optimal conditions, the absorbance values of ALP solutions with different ALP concentrations were measured; the absorption signals were linear with the ALP activities observed within the range of 0–40 mU/mL (Figure 4B) ($Y = 0.010X + 0.146$, $R^2 = 0.993$) and the limit of detection (LOD) for ALP was 0.26 mU/mL evaluated using a signal three-fold the background noise ($S/N = 3$), and a LOQ of 0.30 mU/mL at three times background noise is measured. The ALP activity detection established by this method was better than previously reported, as listed in Table 2.

Table 2. Comparison of our method with other ALP detection methods.

Material	Method	Linear Range (mU/mL)	LOD (mU/mL)	References
Au NPs/ATP	Colorimetric	100–600	10	[51]
Au nanorods	Colorimetric	5–100	3.3	[14]
CdTe/CdS QDs	Fluorescent	3–1000	3	[52]
CDs	Fluorescent	2.5–40	1	[53]
GQDs	Fluorescent	16.7–782.6	1.1	[54]
Protein stabilized gold nanocubes	Fluorescent	0.0312–1	1.616	[55]
PDA nanodots	Colorimetric	1–50	0.94	[56]
His@AuNCs/GO	Colorimetric	0–40	0.26	This work

The assay method we proposed can distinguish the color change caused by ALP with the naked eye, is easy to implement, and meets the sensitivity requirements, and this method does not require expensive instruments to detect ALP [47]. To evaluate the selectivity of the proposed method, an investigation on the influence of potentially interfering substances, including ATP, ADP, AMP, Pi, F^- , Cl^- , Br^- , I^- , SO_4^{2-} , NO_3^- , PO_4^{3-} , CO_3^{2-} , Thr, Val, Pro, His, Leu, and Lys, was performed under the optimized conditions. We observed that the abovementioned coexisting interfering substances had a negligible effect on the absorption intensity (Figure 4C). The results demonstrate that, due

to the strong coordination interaction between PPI and His@AuNCs/GO and the specific catalytic activity of ALP on PPI, the selectivity of the sensor was satisfactory.

The robustness of the proposed method was evaluated by the relative standard deviation (RSD) of sensing affect the His@AuNCs/GO to ALP activity. The results of detection from His@AuNCs/GO of different synthetic batches under the same conditions were shown in Figure S10A. The calculated RSD were 2.57%, indicating the proposed method has good accuracy. In addition, the stability of His@AuNCs/GO was evaluated. The His@AuNCs/GO was stored at 4 °C for one month; afterwards, 95% of the oxidase-like activity of His@AuNCs/GO was still preserved compared with the initial value, and the sensing properties of His@AuNCs/GO to ALP did not change significantly (Figure S10B). These results indicated that the proposed method have good repeatability and outstanding stability.

3.5. Analytical Application in Real Samples

To assess the potential applicability of the method, we conducted an assay of the ALP activity in serum samples with different ALP concentrations. As shown in Table 3, the recovery efficiency and RSD values were obtained in the range of 98.67–102.5% and 2.08–4.44%, respectively, for different samples, indicating the effectiveness and reliability in the application of the proposed His@AuNCs/GO hybrid-based colorimetric assay in real biological samples.

Table 3. Reliability of His@AuNCs/GO for ALP activity detection in real samples ($n = 3$).

Sample	Added (mU/mL)	Detected (mU/mL)	RSD (% , $n = 3$)	Recovery (%)
1	3	2.96	3.22	98.67
2	4	3.97	4.44	99.17
3	6	6.15	2.08	102.50
4	9	9.15	2.24	101.70

4. Conclusions

In summary, we proposed a facile colorimetric assay for the sensitive and selective determination of the ALP activity based on the PPI-inhibited oxidase mimic activity of His@AuNCs/GO. The hydrolysis of PPI by ALP restored the inhibited activity of His@AuNCs/GO, enabling His@AuNCs/GO to efficiently catalyze the oxidation of TMB to generate the blue product oxTMB. The intensity of the color showed a linear dependency (0–40 mU/mL) and can be related to the ALP activity. This is a fast, robust, simple, and cost-effective method that can be used to accurately and reliably detect ALP activity in real samples, which suggests that it has good practicability and reliability in detecting ALP activity in clinical practice.

Supplementary Materials: The following are available online at <https://www.mdpi.com/article/10.3390/bios11060174/s1>, Electronic supplementary information (ESI) available. Figure S1: UV-Vis absorption spectra of His@AuNCs/GO-TMB system with different incubation ratios of His@AuNCs and PDDA-GO (from a to f: 1:10, 1:20, 1:30, 1:40, 1:50, 1:100), Figure S2: UV-Vis absorption spectra of His@AuNCs/GO-TMB system in different concentrations of His@AuNCs/GO (from a to e: 0.002, 0.003, 0.004, 0.005, 0.006 mg/mL), Figure S3: Effect of pH (a), acetate buffer (b) and TMB concentration on the oxidase-like activity of His@AuNCs/GO, Figure S4: The absorbance of the sensing system as a function of the enzymatic reaction time (0, 5, 10, 15, 20, 25, 30, 40, 60 min) in the presence of 0, 10, and 20 mU/mL ALP individually, with PPI as the substrate, Figure S5: The size statistical histograms of His@AuNCs, Figure S6: EDX of His@AuNCs (A), GO (B) and His@AuNCs/GO (C), Figure S7: The absorbance of the sensing His@AuNCs-TMB system with PPI as the substrate, The inset is the inhibitory effect of PPI on His@AuNCs/GO-TMB system, Figure S8: Comparison of the UV-Vis absorption spectra of the His@AuNCs/GO-TMB system after 5 min of reaction with PPI and without PPI, Figure S9: UV-vis absorption spectra of His@AuNCs/GO-TMB system in the presence of ALP and Pi, Figure S10 (A): Detection of ALP activity by colorimetric sensor established by different

batches of His@AuNCs/GO, (B): a represents the oxidase-like activity of His@AuNCs/GO, b and c respectively represent the detection of PPI and ALP by the sensor.

Author Contributions: Writing—original draft preparation, F.X. and Y.Y.; writing—review and editing, Y.W.; investigation, validation, and supervision, L.T., G.Z. and H.P.; conceptualization, J.D. All authors have read and agreed to the published version of the manuscript.

Funding: This research was funded by the National Natural Sciences Foundation of China, grant number: 21565020.

Institutional Review Board Statement: Not applicable.

Informed Consent Statement: Not applicable.

Data Availability Statement: The data presented in this study are available on request from the corresponding author.

Conflicts of Interest: The authors declare no conflict of interest.

References

1. Fernley, H.N. 18 Mammalian Alkaline Phosphatases. In *Enzymes*; Academic Press: Cambridge, MA, USA, 1971; pp. 417–447. [[CrossRef](#)]
2. Coleman, J.E. Structure and mechanism of alkaline phosphatase. *Annu. Rev. Biophys. Biomol. Struct.* **1992**, *21*, 441–483. [[CrossRef](#)]
3. Couttenye, M.M.; D’Haese, P.C.; Van, H.V.O.; Lemoniatou, E.; Goodman, W.; Verpooten, G.A.; De, B.M.E. Low serum levels of alkaline phosphatase of bone origin: A good marker of adynamic bone disease in haemodialysis patients. *Nephrol. Dial. Transplant.* **1996**, *11*, 1065–1072. [[CrossRef](#)]
4. Lorente, J.A.; Valenzuela, H.; Morote, J.; Gelabert, A. Serum bone alkaline phosphatase levels enhance the clinical utility of prostate specific antigen in the staging of newly diagnosed prostate cancer patients. *Eur. J. Nucl. Med.* **1999**, *26*, 625–632. [[CrossRef](#)]
5. Rao, G.M.; Morghom, L.O. Correlation between serum alkaline phosphatase activity and blood glucose levels. *Enzyme* **1986**, *35*, 57. [[CrossRef](#)]
6. Ooi, K.; Shiraki, K.; Morishita, Y.; Nobori, T. High-molecular intestinal alkaline phosphatase in chronic liver diseases. *J. Clin. Lab. Anal.* **2007**, *21*, 133–139. [[CrossRef](#)] [[PubMed](#)]
7. Nistor, C.; Emnéus, J. An enzyme flow immunoassay using alkaline phosphatase as the label and a tyrosinase biosensor as the label detector. *Anal. Commun.* **1998**, *35*, 417–419. [[CrossRef](#)]
8. Ruan, C.; Wang, W.; Gu, B. Detection of alkaline phosphatase using surface-enhanced Raman spectroscopy. *Anal. Chem.* **2006**, *78*, 3379–3384. [[CrossRef](#)]
9. Wang, D.E.; Gao, X.; Li, G.; Xue, T.; Yang, H.; Xu, H. Facile colorimetric assay of alkaline phosphatase activity using polydiacetylene liposomes with calcium ions and pyrophosphate. *Sens. Actuators B Chem.* **2019**, *289*, 85–92. [[CrossRef](#)]
10. Liu, Y.; Xiong, E.; Li, X.; Li, J.; Zhang, X.; Chen, J. Sensitive electrochemical assay of alkaline phosphatase activity based on TdT-mediated hemin/G-quadruplex DNAzyme nanowires for signal amplification. *Biosens. Bioelectron.* **2017**, *87*, 970–975. [[CrossRef](#)]
11. Wu, Z.; Zhou, C.H.; Pan, L.J.; Zeng, T.; Zhu, L.; Pang, D.W.; Zhang, Z.L. Reliable Digital Single Molecule Electrochemistry for Ultrasensitive Alkaline Phosphatase Detection. *Anal. Chem.* **2016**, *88*, 9166–9172. [[CrossRef](#)] [[PubMed](#)]
12. Hayat, A.; Andreescu, S. Nanoceria Particles As Catalytic Amplifiers for Alkaline Phosphatase Assays. *Anal. Chem.* **2013**, *85*, 10028–10032. [[CrossRef](#)]
13. Zhang, L.; Zhao, J.; Duan, M.; Zhang, H.; Jiang, J.; Yu, R. Inhibition of dsDNA-Templated Copper Nanoparticles by Pyrophosphate as a Label-Free Fluorescent Strategy for Alkaline Phosphatase Assay. *Anal. Chem.* **2013**, *85*, 3797–3801. [[CrossRef](#)]
14. Gao, Z.; Deng, K.; Wang, X.D.; Miró, M.; Tang, D. High-resolution colorimetric assay for rapid visual readout of phosphatase activity based on gold/silver core/shell nanorod. *ACS Appl. Mater. Interfaces* **2014**, *6*, 18243–18250. [[CrossRef](#)]
15. Jiao, H.; Chen, J.; Li, W.; Wang, F.; Zhou, H.; Li, Y.; Yu, C. Nucleic Acid-Regulated Perylene Probe-Induced Gold Nanoparticle Aggregation: A New Strategy for Colorimetric Sensing of Alkaline Phosphatase Activity and Inhibitor Screening. *ACS Appl. Mater. Interfaces* **2014**, *6*, 1979–1985. [[CrossRef](#)]
16. Whyte, M.P. Hypophosphatasia—Aetiology, nosology, pathogenesis, diagnosis and treatment. *Nat. Rev. Endocrinol.* **2016**, *12*, 233. [[CrossRef](#)]
17. Babson, A.L.; Greeley, S.J.; Coleman, C.M.; Phillips, G.E. Phenolphthalein Monophosphate as a Substrate for Serum Alkaline Phosphatase. *Clin. Chem.* **1966**, *12*, 482–490. [[CrossRef](#)] [[PubMed](#)]
18. Wang, J.; Ni, P.; Chen, C.; Jiang, Y.; Zhang, C.; Wang, B.; Cao, B.; Lu, Y. Colorimetric determination of the activity of alkaline phosphatase by exploiting the oxidase-like activity of palladium cube@CeO₂ core-shell nanoparticles. *Microchim. Acta* **2020**, *187*. [[CrossRef](#)] [[PubMed](#)]
19. Zhang, Z.; Chen, Z.; Wang, S.; Cheng, F.; Chen, L. Iodine-Mediated Etching of Gold Nanorods for Plasmonic ELISA Based on Colorimetric Detection of Alkaline Phosphatase. *ACS Appl. Mater. Interfaces* **2015**, *7*, 27639–27645. [[CrossRef](#)] [[PubMed](#)]

20. Guo, Y.; Wu, J.; Li, J.; Ju, H. A plasmonic colorimetric strategy for biosensing through enzyme guided growth of silver nanoparticles on gold nanostars. *Biosens. Bioelectron.* **2016**, *78*, 267–273. [[CrossRef](#)]
21. Chen, Y.; Li, W.Y.; Wang, Y.; Yang, X.D.; Chen, J.; Jiang, Y.N.; Yu, C.; Lin, Q. Cysteine-directed fluorescent gold nanoclusters for the sensing of pyrophosphate and alkaline phosphatase. *J. Mater. Chem. C* **2014**, *2*, 4080–4085. [[CrossRef](#)]
22. Zhang, J.; Zhang, C.L.; Yu, S.H. Tuning Gold Nanoparticle Aggregation through the Inhibition of Acid Phosphatase Bioactivity: A Plasmonic Sensor for Light-Up Visual Detection of Arsenate (As-V). *ChemPlusChem* **2016**, *81*, 1147–1151. [[CrossRef](#)] [[PubMed](#)]
23. Chen, Q.; Li, S.; Liu, Y.; Zhang, X.; Tang, Y.; Chai, H.; Huang, Y. Size-controllable Fe-N/C single-atom nanozyme with exceptional oxidase-like activity for sensitive detection of alkaline phosphatase. *Sens. Actuators B Chem.* **2020**, *305*. [[CrossRef](#)]
24. Lin, Z.; Zhang, X.; Liu, S.; Zheng, L.; Bu, Y.; Deng, H.; Chen, R.; Peng, H.; Lin, X.; Chen, W. Colorimetric acid phosphatase sensor based on MoO₃ nanozyme. *Anal. Chim. Acta* **2020**, *1105*, 162–168. [[CrossRef](#)] [[PubMed](#)]
25. Tian, F.; Zhou, J.; Ma, J.; Liu, S.; Jiao, B.; He, Y. MnO₂ nanosheets as oxidase mimics for colorimetric detection of alkaline phosphatase activity. *Microchim. Acta* **2019**, *186*. [[CrossRef](#)]
26. Chen, C.X.; Zhao, D.; Jiang, Y.Y.; Ni, P.J.; Zhang, C.H.; Wang, B.; Yang, F.; Lu, Y.Z.; Sun, J. Logically Regulating Peroxidase-Like Activity of Gold Nanoclusters for Sensing Phosphate-Containing Metabolites and Alkaline Phosphatase Activity. *Anal. Chem.* **2019**, *91*, 15017–15024. [[CrossRef](#)]
27. Wang, C.H.; Gao, J.; Cao, Y.L.; Tan, H.L. Colorimetric logic gate for alkaline phosphatase based on copper (II)-based metal-organic frameworks with peroxidase-like activity. *Anal. Chim. Acta* **2018**, *1004*, 74–81. [[CrossRef](#)]
28. Fan, S.; Jiang, X.; Yang, M.; Wang, X. Sensitive colorimetric assay for the determination of alkaline phosphatase activity utilizing nanozyme based on copper nanoparticle-modified Prussian blue. *Anal. Bioanal. Chem.* **2021**, 1–9. [[CrossRef](#)]
29. Xie, X.; Wang, Y.; Zhou, X.; Chen, J.; Wang, M.; Su, X. Fe—C single-atom nanozymes with peroxidase-like activity for the detection of alkaline phosphatase. *Analyst* **2021**, *146*, 896–903. [[CrossRef](#)]
30. Hou, Y.; Lu, Y.; Chen, Q.; Zhang, X.; Huang, Y. Ultrathin two-dimensional carbon nanosheets with highly active Cu-N_x sites as specific peroxidase mimic for determining total antioxidant capacity. *Sens. Actuators B Chem.* **2021**, *333*, 129549. [[CrossRef](#)]
31. Adegoke, O.; Zolotovskaya, S.; Abdolvand, A.; Daeid, N.N. Rapid and highly selective colorimetric detection of nitrite based on the catalytic-enhanced reaction of mimetic Au nanoparticle-CeO₂ nanoparticle-graphene oxide hybrid nanozyme. *Talanta* **2021**, *224*, 121875. [[CrossRef](#)]
32. Nana, L.; Ruiyi, L.; Qinsheng, W.; Yongqiang, Y.; Xiulan, S.; Guangli, W.; Zaijun, L. Colorimetric detection of chlorpyrifos in peach based on cobalt-graphene nanohybrid with excellent oxidase-like activity and reusability. *J. Hazard. Mater.* **2021**, *415*, 125752. [[CrossRef](#)]
33. Xue, Q.; Li, X.; Peng, Y.; Liu, P.; Peng, H.; Niu, X. Polyethylenimine-stabilized silver nanoclusters act as an oxidoreductase mimic for colorimetric determination of chromium(VI). *Microchim. Acta* **2020**, *187*. [[CrossRef](#)]
34. Zhang, T.; Zhang, S.; Liu, J.; Li, J.; Lu, X. Efficient visual Chemosensor for Hexavalent Chromium via a Controlled Strategy for Signal Amplification in Water. *Anal. Chem.* **2020**, *92*, 3426–3433. [[CrossRef](#)] [[PubMed](#)]
35. Wu, N.; Wang, Y.-T.; Wang, X.-Y.; Guo, F.-N.; Wen, H.; Yang, T.; Wang, J.-H. Enhanced peroxidase-like activity of AuNPs loaded graphitic carbon nitride nanosheets for colorimetric biosensing. *Anal. Chim. Acta* **2019**, *1091*, 69–75. [[CrossRef](#)]
36. Chen, M.M.; Yang, B.C.; Zhu, J.L.; Liu, H.; Zhang, X.; Zheng, X.W.; Liu, Q.Y. FePt nanoparticles-decorated graphene oxide nanosheets as enhanced peroxidase mimics for sensitive response to H₂O₂. *Mater. Sci. Eng. C Mater. Biol. Appl.* **2018**, *90*, 610–620. [[CrossRef](#)]
37. Liu, L.; Du, J.; Liu, W.-E.; Guo, Y.; Wu, G.; Qi, W.; Lu, X. Enhanced His@AuNCs oxidase-like activity by reduced graphene oxide and its application for colorimetric and electrochemical detection of nitrite. *Anal. Bioanal. Chem.* **2019**, *411*, 2189–2200. [[CrossRef](#)]
38. Ren, W.; Fang, Y.; Wang, E. A Binary Functional Substrate for Enrichment and Ultrasensitive SERS Spectroscopic Detection of Folic Acid Using Graphene Oxide/Ag Nanoparticle Hybrids. *ACS Nano* **2011**, *5*, 6425–6433. [[CrossRef](#)] [[PubMed](#)]
39. Hu, L.; Liao, H.; Feng, L.; Wang, M.; Fu, W. Accelerating the Peroxidase-Like Activity of Gold Nanoclusters at Neutral pH for Colorimetric Detection of Heparin and Heparinase Activity. *Anal. Chem.* **2018**, *90*, 6247–6252. [[CrossRef](#)] [[PubMed](#)]
40. Liu, W.; Tian, L.; Du, J.; Wu, J.; Liu, Y.; Wu, G.; Lu, X.J.A. Triggered peroxidase-like activity of Au decorated carbon dots for colorimetric monitoring of Hg²⁺ enrichment in *Chlorella vulgaris*. *Analyst* **2020**, *145*, 5500–5507. [[CrossRef](#)]
41. Jiang, X.; Wang, X.; Lin, A.; Wei, H.J.A.C. In Situ Exsolution of Noble-Metal Nanoparticles on Perovskites as Enhanced Peroxidase Mimics for Bioanalysis. *Anal. Chem.* **2021**, *93*, 5954–5962. [[CrossRef](#)]
42. Kargar, S.; Elhamifar, D.; Zarnegaryan, A. Ionic liquid modified graphene oxide supported Mo-complex: A novel, efficient and highly stable catalyst. *Surf. Interfaces* **2021**, *23*, 100946. [[CrossRef](#)]
43. Chaityakun, S.; Witit-Anun, N.; Nuntawong, N.; Chindaudom, P.; Oaew, S.; Kedkeaw, C.; Limsuwan, P. Preparation and characterization of graphene oxide nanosheets. *Procedia Eng.* **2012**, *32*, 759–764. [[CrossRef](#)]
44. Wang, L.; Zhu, L.; Yu, Q.; Chen, S.; Cui, Y.; Sun, H.; Gao, D.; Lan, X.; Yang, Q.; Xiao, H. Polymer Edition. Enhanced glucose detection using dendrimer encapsulated gold nanoparticles benefiting from their zwitterionic surface. *J. Biomater. Sci. Polym. Ed.* **2018**, *29*, 2267–2280. [[CrossRef](#)] [[PubMed](#)]
45. Li, C.M.; Zhen, S.J.; Wang, J.; Li, Y.F.; Huang, C.Z. A gold nanoparticles-based colorimetric assay for alkaline phosphatase detection with tunable dynamic range. *Biosens. Bioelectron.* **2013**, *43*, 366–371. [[CrossRef](#)] [[PubMed](#)]
46. Ren, X.; Chen, Z.; Chen, X.; Liu, J.; Tang, F. Sensitive optical detection of alkaline phosphatase activity with quantum dots. *J. Lumin.* **2014**, *145*, 330–334. [[CrossRef](#)]

47. Kang, W.; Ding, Y.; Zhou, H.; Liao, Q.; Yang, X.; Yang, Y.; Jiang, J.; Yang, M. Monitoring the activity and inhibition of alkaline phosphatase via quenching and restoration of the fluorescence of carbon dots. *Microchim. Acta* **2015**, *182*, 1161–1167. [[CrossRef](#)]
48. Qian, Z.S.; Chai, L.J.; Huang, Y.Y.; Tang, C.; Jia Shen, J.; Chen, J.R.; Feng, H. A real-time fluorescent assay for the detection of alkaline phosphatase activity based on carbon quantum dots. *Biosens. Bioelectron.* **2015**, *68*, 675–680. [[CrossRef](#)] [[PubMed](#)]
49. Sharma, A.K.; Pandey, S.; Khan, M.S.; Wu, H.F. Protein stabilized fluorescent gold nanocubes as selective probe for alkaline phosphatase via inner filter effect. *Sens. Actuators B Chem.* **2018**, *259*, 83–89. [[CrossRef](#)]
50. Xue, Q.; Cao, X.; Zhang, C.; Xian, Y. Polydopamine nanodots are viable probes for fluorometric determination of the activity of alkaline phosphatase via the in situ regulation of a redox reaction triggered by the enzyme. *Microchim. Acta* **2018**, *185*, 1–9. [[CrossRef](#)]
51. Yang, H.K.; Xiao, J.Y.; Su, L.; Feng, T.; Lv, Q.Y.; Zhang, X.J. Oxidase-mimicking activity of the nitrogen-doped Fe₃C@C composites. *Chem. Commun.* **2017**, *53*, 3882–3885. [[CrossRef](#)]
52. Deng, H.H.; Lin, X.L.; Liu, Y.H.; Li, K.L.; Zhuang, Q.Q.; Peng, H.P.; Liu, A.L.; Xia, X.H.; Chen, W. Chitosan-stabilized platinum nanoparticles as effective oxidase mimics for colorimetric detection of acid phosphatase. *Nanoscale* **2017**, *9*, 10292–10300. [[CrossRef](#)]
53. Qin, L.; Wang, X.; Liu, Y.; Wei, H. 2D-Metal–Organic-Framework-Nanozyme Sensor Arrays for Probing Phosphates and Their Enzymatic Hydrolysis. *Anal. Chem.* **2018**, *90*, 9983–9989. [[CrossRef](#)] [[PubMed](#)]
54. Hou, L.; Qin, Y.; Li, J.; Qin, S.; Huang, Y.; Lin, T.; Guo, L.; Ye, F.; Zhao, S. A ratiometric multicolor fluorescence biosensor for visual detection of alkaline phosphatase activity via a smartphone. *Biosens. Bioelectron.* **2019**, *143*, 111605. [[CrossRef](#)] [[PubMed](#)]
55. Muthuraj, B.; Mukherjee, S.; Chowdhury, S.R.; Patra, C.R.; Iyer, P.K. An efficient strategy to assemble water soluble histidine-perylene diimide and graphene oxide for the detection of PPI in physiological conditions and in vitro. *Biosens. Bioelectron.* **2017**, *89*, 636–644. [[CrossRef](#)] [[PubMed](#)]
56. Zhou, Q.; Lin, Y.X.; Xu, M.D.; Gao, Z.Q.; Yang, H.H.; Tang, D.P. Facile Synthesis of Enhanced Fluorescent Gold-Silver Bimetallic Nanocluster and Its Application for Highly Sensitive Detection of Inorganic Pyrophosphatase Activity. *Anal. Chem.* **2016**, *88*, 8886–8892. [[CrossRef](#)] [[PubMed](#)]